

# Extremum-Seeking Control of a Mode-Locked Laser

Steven L. Brunton\*, Xing Fu, and J. Nathan Kutz  
Applied Mathematics, University of Washington, Seattle, WA 98195

**Abstract**—An adaptive controller is demonstrated that is capable of both obtaining and maintaining high-energy, single-pulse states in a mode-locked fiber laser. In particular, a multi-parameter extremum-seeking control (ESC) algorithm is used on a nonlinear polarization rotation (NPR) based laser using waveplate and polarizer angles to achieve optimal passive mode-locking despite large disturbances to the system. The physically realizable objective function introduced divides the energy output by the kurtosis of the pulse spectrum, thus balancing the total energy with the coherence of the mode-locked solution. Moreover, its peaks are high-energy mode-locked states that have a safety margin near parameter regimes where mode-locking breaks down or the multi-pulsing instability occurs. The extremum seeking controller is demonstrated by numerical simulations of a single-NPR mode-locked laser and is able to track locally maximal mode-locked states despite significant disturbances to parameters such as the fiber birefringence.

**Index Terms**— Mode locked laser, fiber laser, nonlinear polarization rotation, adaptive control, feedback control, extremum seeking control.

## I. INTRODUCTION

Mode-locked lasers are characterized by the locking of multiple axial modes in the laser cavity, thus resulting in resonant, ultrashort pulsing phenomenon [14, 22, 37, 38, 40, 39]. Over the past decades, such mode-locked lasers have become commercially and scientifically successful, impacting medical imaging [18], two-photon microscopy [8, 47], femtosecond chemistry [48], micro-machining [15, 27], surgery [17, 44, 42, 43], and fusion research [12], for instance. Fiber-based mode-locked lasers are particularly interesting due to the numerous inherent advantages of the optical fiber platform [40]. Recent trends have shown that these fiber-based lasers may eventually achieve competitive performance with their solid-state counterparts [40, 2], thus potentially shifting the field of ultra-fast, high-power lasers to fiber based technologies. Closing the order of magnitude performance gap between fiber and solid-state lasers will require the ability to control and optimize laser cavity output energy and pulse-width. This motivates the extremum-seeking control advocated here whereby optimal cavity performance can be achieved even with a large parameter space and the effects of considerable perturbations to the cavity.

One of the most prolific and dominant fiber-based mode-locking lasers demonstrated to date involves a linear polarizer

and a number of waveplates to achieve saturable absorption via nonlinear polarization rotation (NPR) [14, 23, 33, 10]. Such passive mode-locking is compact, comparatively inexpensive, reliable, and requires less optical tuning compared with alternative ultrafast laser technologies. However, the multi-pulsing instability (MPI) imposes a fundamental performance limit on the mode-locked laser cavity, thus preventing fiber lasers from achieving the desired solid-state performance levels [20]. To overcome MPI, it was recently demonstrated that two (or more) NPR sections (dual transmission filters) could increase the pulse energy output [25] by circumventing MPI at high gains [32, 3, 11, 26]. Combined with the recent experimental demonstration of electronic control of waveplates and polarizer [41], a genetic algorithm could be implemented to search through the high-dimensional parameter space for multiple-NPR lasers in order to find high-energy mode-locked solutions [13].

Even with such potential advancements, it remains challenging and expensive to find high-energy, single-pulse solutions in the multiple-NPR case. Moreover, even if mode-locking is achieved, it may be destroyed by changes to the birefringence [29, 30], which often varies throughout the day and may change abruptly if the laser system is physically perturbed [19]. This requires commercial lasers based upon NPR, for instance, to enforce strict environmental control in order to maintain performance, i.e. the fiber is pinned into place and protected from temperature fluctuations.

Alternatively, feedback control promises significant performance enhancements, including maintaining high-energy, mode-locked pulses despite large variations in parameters (e.g., birefringence, thermal/optical, etc.), as suggested in [40]. However, feedback control typically involves a detailed model of the underlying dynamics, and many of the most powerful tools only apply to linear or nearly-linear systems. In the mode-locked laser, the underlying dynamics are strongly nonlinear, and the variation with respect to parameters is difficult to model. In particular, the fiber birefringence lacks a precise, quantitatively accurate model for its fluctuations and dependence on bending, temperature, etc.

Extremum-seeking control (ESC) is an adaptive method of finding local maxima of an objective function on the output of a dynamical system that bypasses many of the aforementioned issues. The controller does not require a model of the underlying dynamics, which is advantageous for complex, nonlinear systems with parameter dependence that is difficult to model, such as the laser cavity birefringence, which can

\* Corresponding author. Tel.: +1 206 685 3037.  
E-mail address: sbrunton@uw.edu (S.L. Brunton).

easily corrupt performance. Extremum-seeking has recently been made mathematically rigorous [1, 21, 7], and stability guarantees have been proven under certain conditions.

Extremum-seeking control has been applied to a wide range of problems, including maximum-power point tracking for photovoltaic power optimization [24, 5, 6] and wind turbine optimization [31], reducing the noise of a jet [28], active shear layer control for drag reduction in fluids [35], maximizing the pressure rise in an axial flow compressor [46], optimizing bioreactors [45], controlling the current profile in a Tokamak [34], and in active braking systems for automobiles [49]. The above examples involve a single control variable, using what is known as *single-parameter* extremum seeking. Multi-parameter extremum seeking, involving the simultaneous control of multiple inputs, has been applied to the problem of formation flight [4], and also to laser pulse shaping [36].

In this paper, we apply multi-parameter extremum seeking control to find and maintain locally optimal single-pulse laser solutions. A single-NPR cavity laser is simulated according to the model described in Section II, and a new objective function is developed in Section III that has high-energy mode-locked pulses as local maxima. The extremum-seeking control architecture is described in Section IV. Section V contains the numerical results demonstrating the effectiveness of the adaptive controller both to find local maxima for fixed birefringence, and to track these high-energy, single-pulse solutions when the birefringence is varying. The variations in birefringence may be viewed as a general disturbance to the system, either due to thermal fluctuations, or physical perturbations to the laser system. The results are summarized in Section VI, and future directions are discussed, including the extension of these methods to multiple-NPR cavities in experiments.

## II. MODEL OF SINGLE-NPR MODE-LOCKED LASER

A schematic of the laser is shown in Figure 1. We model the laser by describing the intra-cavity pulse evolution in a component by component manner. Thus the nonlinear propagation in the optical fiber is treated separately from the discretely applied waveplates and polarizer each round trip through the cavity. This treatment is discussed in detail in [10].

### A. Coupled Nonlinear Schrödinger Equations

The optical field propagation in the fiber are well-described by the coupled nonlinear Schrödinger equations (CNLS) [29, 30]:

$$\begin{aligned} i \frac{\partial z}{\partial u} + \frac{D}{2} \frac{\partial^2 u}{\partial t^2} - Ku + (|u|^2 + A|v|^2)u + Bv^2u^* &= iRu, \\ i \frac{\partial z}{\partial v} + \frac{D}{2} \frac{\partial^2 v}{\partial t^2} + Kv + (A|u|^2 + |v|^2)v + Bu^2v^* &= iRv. \end{aligned} \quad (1)$$

In the above equations,  $u(z, t)$  and  $v(z, t)$  are the two orthogonally polarized electric field envelopes in an optical fiber.  $t$  is time non-dimensionalized by the full-width at half-maximum of the pulse, and  $z$  is the propagation distance normalized by the cavity length. The functions  $u$  and  $v$  are often referred to as the fast and slow components, respectively.  $K$  is the

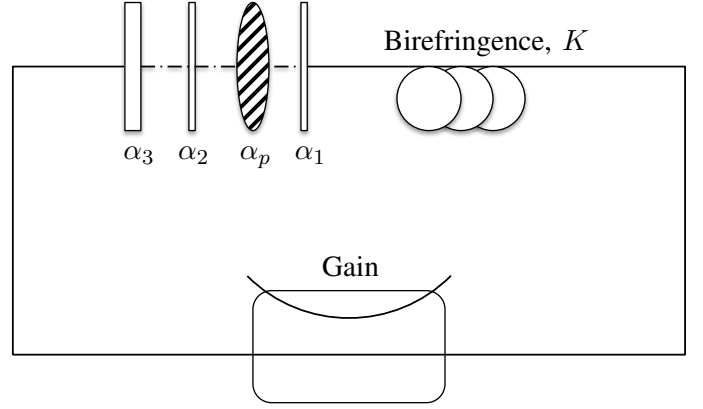


Fig. 1. Schematic of mode-locked laser with passive nonlinear polarization rotation (NPR). The quarter-waveplate angles are  $\alpha_1$  and  $\alpha_2$ , the half-waveplate angle is  $\alpha_3$ , and  $\alpha_p$  is the angle of the polarizer. There is additionally the birefringence parameter  $K$  that arises due to the fiber geometry and its material properties.

birefringence,  $D$  is the average group velocity dispersion of the cavity. The nonlinear coupling parameters  $A$  and  $B$  correspond to the cross-phase modulation and the four-wave mixing, respectively. They are determined by physical properties of the fiber, and  $A + B = 1$ . For this case (a silica fiber),  $A = 2/3$  and  $B = 1/3$ . The dissipative terms  $Ru$  and  $Rv$  account for the saturable, bandwidth-limited gain and attenuation arising from the Yb-doped amplification. The operator  $R$  is given by

$$R = \frac{2g_0 (1 + \tau \partial_t^2)}{1 + (1/e_0) \int_{-\infty}^{\infty} (|u|^2 + |v|^2) dt} - \Gamma,$$

where  $g_0$  is the non dimensional-pumping strength, and  $e_0$  is the non-dimensional saturating energy of the gain medium. The pump bandwidth is  $\tau$  and  $\Gamma$  quantifies losses due to output coupling and fiber attenuation.

### B. Jones Matrices for Waveplates and Polarizers

The application of the waveplates and passive polarizer after each round trip through the cavity may be modeled by the discrete application of Jones matrices [16, 20, 9]:

$$W_{\lambda/4} = \begin{bmatrix} e^{-i\pi/4} & 0 \\ 0 & e^{i\pi/4} \end{bmatrix}, W_{\lambda/2} = \begin{bmatrix} -i & 0 \\ 0 & i \end{bmatrix}, W_p = \begin{bmatrix} 1 & 0 \\ 0 & 0 \end{bmatrix}.$$

Here,  $W_{\lambda/4}$  is the quarter-waveplate ( $\alpha_1$  and  $\alpha_2$ ),  $W_{\lambda/2}$  is the half-waveplate ( $\alpha_3$ ), and  $W_p$  is the polarizer ( $\alpha_p$ ). If the principle axes of these objects are not aligned with the fast field of the cavity, it is necessary to include the addition of a rotation matrix:

$$J_j = R(\alpha_j)W_jR(-\alpha_j), \quad R(\alpha_j) = \begin{bmatrix} \cos(\alpha_j) & -\sin(\alpha_j) \\ \sin(\alpha_j) & \cos(\alpha_j) \end{bmatrix},$$

where  $\alpha_j$  is a waveplate or polarizer angle ( $j = 1, 2, 3, p$ ). These rotation angles will be the control variables, allowing us to find mode-locked solutions. Recent experiments show that these control variables can be easily manipulated through electronic control [41].

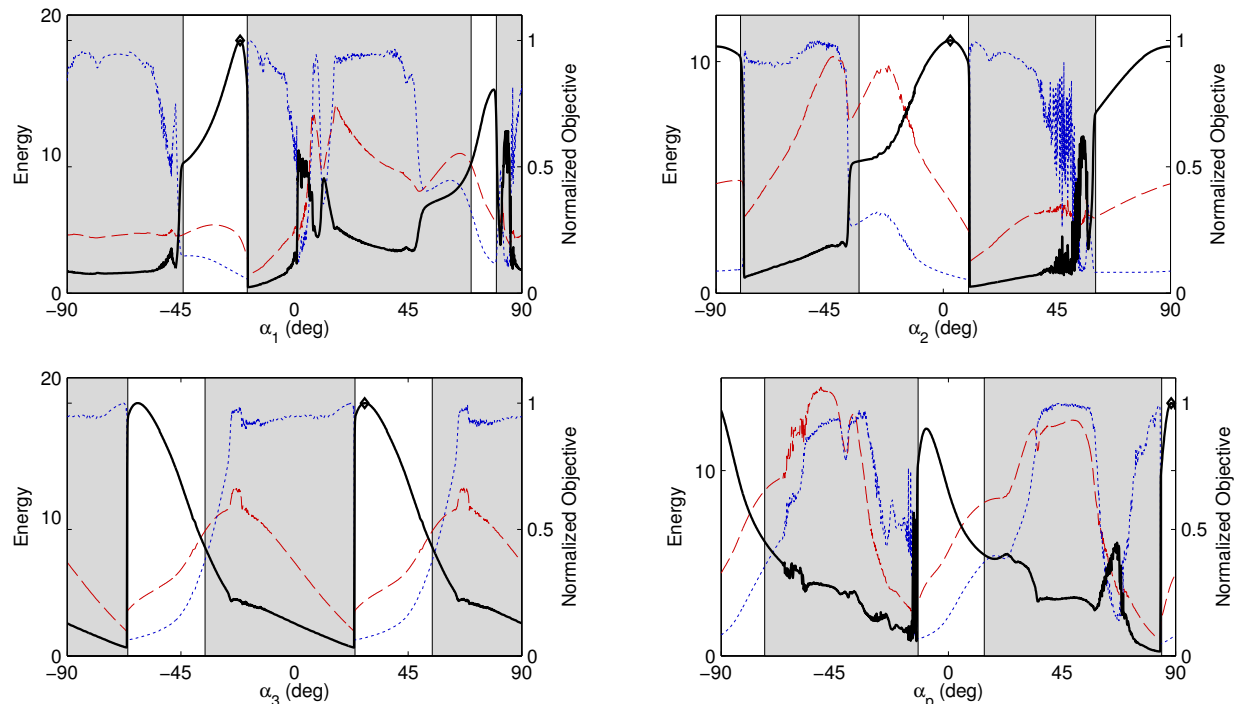


Fig. 2. Objective function  $E/\kappa$  (solid black), energy  $E$  (dashed red) and kurtosis of the spectrum  $\kappa$  (blue dots) for varying waveplate and polarizer rotation angles  $\alpha_1, \alpha_2, \alpha_3$  and  $\alpha_p$ . Single-pulse mode-locking occurs in the white regions. As each angle is varied, all other angles are held fixed at locally maximizing values, indicated by black diamonds.

TABLE I  
SINGLE-NPR COMPUTATIONAL PARAMETERS

$\tau$	$\Gamma$	$A$	$B$	$D$	$K$	$g_0$	$e_0$	$L_t$	$N_t$
0.1	0.1	2/3	1/3	-0.4	0.1	1.73	4.23	60	256

### C. Numerical Integration Scheme

The CNLS equations are solved in the spectral domain by using the fast Fourier transform (FFT) along with an adaptive-step, fourth-order Runge-Kutta scheme to integrate initial conditions one round trip through the cavity. The Jones matrices are then applied to model the discrete application of waveplates and polarizer, and the entire process is repeated. Mode-locking spontaneously arises from white-noise initial conditions after a short number of round trips. The numerics used in this work are an extension of the methods developed in [10, 13]. Typical parameters used in these simulations are given in Table I. The round-trip length is 1.5 dimensionless units.

## III. OBJECTIVE FUNCTION

For any extremum-seeking controller to be effective, we require an objective function with local maxima that correspond to high-energy mode-locked solutions. Although we seek high-energy solutions, there are many chaotic waveforms that have significantly higher energy than mode-locked solutions. Therefore, energy alone is not a good objective function. Instead, we divide the energy function ( $E$ ) by the kurtosis ( $\kappa$ ) of the Fourier spectrum of the waveform, which is large for undesirable chaotic solutions. This objective function is large

when we have a large amount of energy in a tightly confined temporal wave packet. The kurtosis of a signal  $x$  is given by the fourth moment about the mean divided by the square of the variance:  $\kappa = E[(x - \bar{x})^4] / E[(x - \bar{x})^2]^2$ .

Figure 2 shows the new objective function (solid black), energy (red dash), and the kurtosis of the spectrum (blue dots) for various slices of the rotation angles  $\alpha_j$ . In each panel, one of the angles is rotated from  $-90^\circ$  to  $90^\circ$  while the other angles are held fixed at values that locally maximize the objective function. These locally optimal values are obtained by applying the extremum-seeking controller developed in the next sections. In each panel, the maximal energy occurs away from the regions of single-pulse mode locking, shown by the white-regions, and tracking energy alone would lead to chaotic solutions (grey regions). In contrast, the new objective function has local maxima in the single-pulse mode-locked regions, and there is a buffer between the peak in objective function and the grey region where mode-locking fails. The white regions are determined manually by checking if the solution has a single pulse. These regions are not used by the control algorithms, but are included to illustrate the regions of stability. The spectral kurtosis (blue dots) is small in the single-pulse mode-locking regions (white) and is much larger in the grey regions because of multi-pulse or chaotic solutions. Thus, dividing energy by the spectral kurtosis penalizes non-mode-locking solutions.

It may be tempting to use an angle that is right at the edge of the white region with higher energy, for example in the third panel in the second white region. These edge points, although they do contain more energy, correspond to fat mode-locked

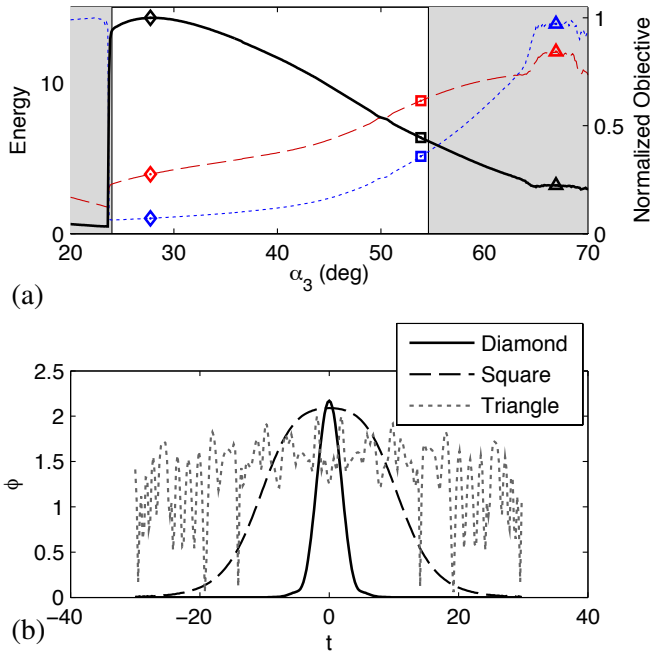


Fig. 3. Zoom in near peak in objective function ( $\diamond$ ). (a) The objective function (—), energy (---), and kurtosis (···) versus half-waveplate angle  $\alpha_3$ . (b) Energy of the waveforms versus time for the cases shown in diamond ( $\diamond$ ), square ( $\square$ ), and triangle ( $\triangle$ ). The peak of the objective function ( $\diamond$ ) is a localized pulse, and the peak of the total energy ( $\triangle$ ) is a chaotic solution.

pulses and are not as favorable as the tight pulses at the peak of the black curves. In addition, being close to the grey boundary makes this solution susceptible to disruption by any manner of disturbance to the system (e.g., birefringence, thermal optical, etc.).

Consider Figure 3, which is a zoom-in of the third panel of Figure 2. As we vary  $\alpha_3$  with all of the other angles held fixed, the energy function increases monotonically in the single-pulse mode-locked regions. An extremum seeking controller maximizing the energy would climb this function past the largest single-pulse energy solution ( $\square$ ) to the peak energy solution ( $\triangle$ ) which is in the middle of the grey region, and is chaotic. In the second panel of Figure 3, we see this chaotic solution ( $\triangle$ ), as well as the fat pulse at the edge of the white region ( $\square$ ), and the desirable tight mode-locked pulse ( $\diamond$ ) that maximizes the new objective function. Table II shows the energy  $E$ , kurtosis of the spectrum  $\kappa$ , and the new objective function  $E/\kappa$  for each of these three cases.

TABLE II  
COMPARISON OF THREE LASER STATES.

	Energy, $E$	Kurtosis, $\kappa$	Objective, $E/\kappa$
Tight Pulse, ( $\diamond$ )	3.9314	17.6153	0.2232
Fat Pulse, ( $\square$ )	8.7932	88.6002	0.0992
Chaotic, ( $\triangle$ )	11.0067	229.2296	0.0480

It is important to note that this objective function is not the only good choice, and others may be more readily deter-

mined from experimental measurements. We have chosen an objective function that balances the total energy in a pulse with some measure of the width of the pulse, which selects for tight mode-locked pulses. However, if a fat pulse is more favorable in a given application, it is possible to construct an objective function for which these waveforms are local maxima. The following control laws will work for any objective function whose local maxima are mode-locked pulses of the desirable shape and characteristics.

#### IV. EXTREMUM-SEEKING CONTROLLER

Extremum-seeking control (ESC) is an adaptive control law that finds and tracks local maxima of an objective function by sinusoidally varying a set of input parameters and measuring the consequent variation of the objective function [21, 7, 1]. The resulting controller does not rely on a model of the dynamics that relate the input parameters to the objective function, making it especially useful for complex, nonlinear systems with disturbances that are difficult to model. Instead, the measured variation in the objective function is compared with the varying input signal to dynamically improve an estimate of the optimal input parameter. If designed correctly, extremum-seeking is guaranteed to stably converge to a neighborhood of the control input  $u^*$  that yields a local maximum of the objective function.

Figure 4 shows an extremum-seeking controller for the laser system with a single-input and a single-output (SISO). The input variable is a single polarizer angle, and the output is the objective function  $E/\kappa$  discussed in Section III. The algorithm works by adding a perturbation signal  $a \sin(\omega t + \beta)$  to the *best guess* of the input  $\hat{u}$  that maximizes the quantity of interest, namely, the objective function. The perturbation passes through the system and results in a perturbation in the output. The high-pass filter of this output is a signal  $\rho$  that oscillates about zero mean. Multiplying the high-pass filtered output by the input perturbation yields a *demodulated* signal  $\xi$  that is positive when  $\hat{u} < u^*$  and negative when  $\hat{u} > u^*$ . Finally, integrating  $\xi$  into our estimate  $\hat{u}$  brings the estimate  $\hat{u}$  closer to the optimal value  $u^*$  corresponding to a local maximum. The input and output sinusoids are plotted with the demodulated signal  $\xi$  in Figure 5.

There are a number of important considerations when designing an extremum-seeking-controller. First, there are three distinct time-scales of interest in the problem:

1. slow - external disturbances to be rejected,
2. medium - perturbation frequency  $\omega$ ,
3. fast - internal system dynamics.

The perturbation frequency  $\omega$  must be chosen to be faster than the external disturbances (such as slow changes in birefringence) and slower than the internal system dynamics. For the laser system, the internal dynamics are extremely fast compared with the time it takes to change the polarizer angles.

Next, the amplitude of the perturbation  $a$  is chosen sufficiently large so that there is a measurable perturbation in the output of the system; larger  $a$  also results in faster convergence

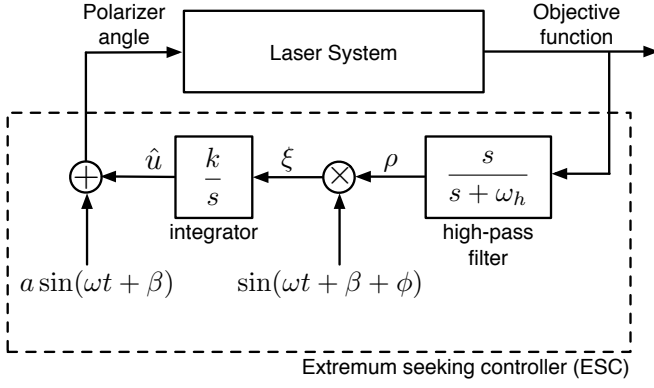


Fig. 4. Single-input, single-output (SISO) extremum-seeking controller.

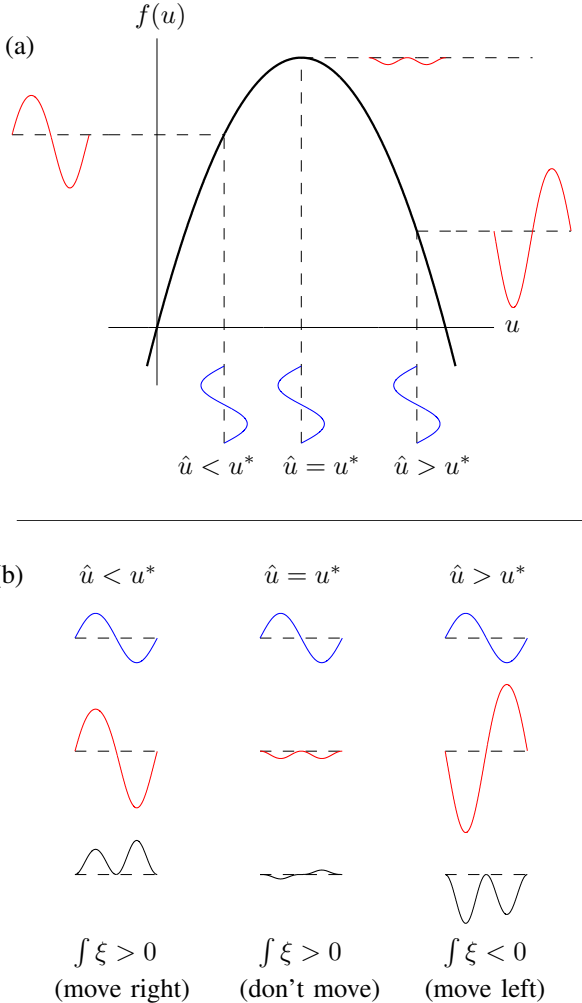


Fig. 5. (a) Illustration of sinusoidal perturbation to the input  $\hat{u}$  near an optimal value  $u^*$ . (b) The input and high-pass filtered outputs are multiplied to give the black curves ( $\xi$ ). If  $\hat{u} < u^*$ , then  $\xi$  is purely positive, and  $\hat{u}$  moves to the right towards  $u^*$ . Similarly, if  $\hat{u} > u^*$  then  $\xi$  is purely negative and  $\hat{u}$  moves left. When  $\hat{u} = u^*$ , then the integral of  $\xi$  is zero, and  $\hat{u}$  doesn't move. Notice that the signal  $\xi$  is larger when the slope of the function is larger.

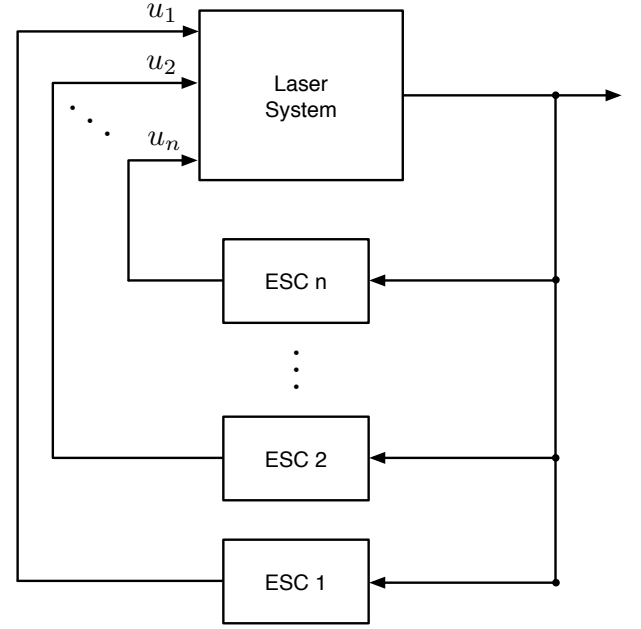


Fig. 6. Schematic for multiple-input, single-output (MISO) extremum-seeking controller. Each ESC block is a SISO unit as shown in Figure 4.

to the optimal  $u^*$ . However,  $a$  should not be so large that there is significant steady-state error due to oscillations about the peak. Faster convergence is also attainable by increasing the integrator gain  $k$ , although this will destabilize the system for large enough  $k$ . Finally, we choose the cut-off frequency  $\omega_h$  for the high-pass filter based on the perturbation frequency  $\omega$ .

Figure 6 shows a multi-parameter extremum-seeking controller for the laser system with multiple-inputs, and a single-output (MISO). This consists of a number of separate extremum-seeking loops (labeled ESC 1 through ESC  $n$ ), each with their own perturbation signal and magnitude, high-pass filter, and integrator. It is generally more involved to develop a well-tuned extremum-seeking controller for a MISO system, although guidelines for stable controllers do exist [1].

The perturbation frequencies of each extremum-seeking loop must satisfy the following property:  $\omega_i + \omega_j \neq \omega_k$  for any  $i, j, k = 1, 2, \dots, n$ . This protects against the possibility of bias arising from demodulation. It is also possible to use the same perturbation frequency for each pair of even and odd controllers, so that  $\omega_k = \omega_{k+1}$  as long as they are out of phase:  $\beta_k = 0$  and  $\beta_{k+1} = \pi/2$ . In practice, we designed each of the single-parameter controllers in isolation and then sequentially combined parameters and refined the design.

It is important to note that the extremum-seeking controller will only find local maxima of the objective function. Therefore, it is important to start with a reasonably good mode-locked solution as the initial condition. One potential way to ensure that good solutions are used in the extremum-seeking controller is to first apply a genetic algorithm to find suitable regions of performance [13]. However, there are also other methods as outlined in the next section.

## V. PERFORMANCE OF EXTREMUM-SEEKING CONTROL

The results in this section demonstrate the utility of extremum-seeking control for the mode-locked laser. In the first two sections, the controller is used to find locally optimal polarizer angles for a fixed birefringence  $K$ . In the third section, the controller is used to track a high-energy mode-locked state despite significant variations in birefringence that occur on the order of minutes. This is designed to be a worst-case scenario to demonstrate the high performance of the controller. It is expected that typical disturbances will be more mild, both in terms of amplitude and frequency of disturbances.

Since the extremum-seeking controller only finds local maxima, there are initial conditions that yield poor locally optimal solutions that are not mode-locked. Similarly, drastic perturbations may knock the system far enough from the local maximum that the controller is unable to recover. We envision a start-up routine to select good initial conditions at the beginning of operation and after drastic perturbations, whereby each of the polarizer/wave-plate angles are varied simultaneously at different, incommensurable rates. This strategy has been tested in simulations, and it is possible to find sub-optimal mode-locked solutions very quickly, within a relatively small number of whole revolutions of the slowest angle. From this starting condition, we then turn the extremum-seeking controller on.

There is no guarantee that the extremum-seeking controller will arrive at the same local maximum, given different initial conditions. In fact, it is impossible to tell if the extremum-seeking controller arrives at the globally maximizing solution without a full parametric study, which may be prohibitively expensive. However, the general approach of cycling each control angle at incommensurable rates is guaranteed to pass arbitrarily close to every possible configuration in a finite amount of time without sampling the same condition twice. This provides a powerful and flexible strategy for mapping configuration space. After a favorable mode-locked solution is found, the extremum-seeking controller is turned on to first obtain and then maintain the local maxima, despite disturbances.

### A. Single-Parameter Extremum-Seeking Control for Fixed Birefringence $K$

Figure 7 shows the extremum-seeking controller for a single-input, single-output (SISO) case. The polarization angle  $\alpha_p$  is the control variable. Both the objective function and the energy rise from the initial value as the controller tracks the (locally) optimal parameter value. Steady-state tracking is achieved within approximately 30 seconds. Although the input parameter continues to oscillate after the extremum is found, the oscillations in the objective function are quite small since the first derivative is zero at the peak. The parameter values of the extremum-seeking controller used in Figure 7 are given in Table III.

Single-parameter extremum-seeking control has also been simulated numerically for the other waveplate angles,  $\alpha_1$ ,  $\alpha_2$ , and  $\alpha_3$  independently, and the results are qualitatively the

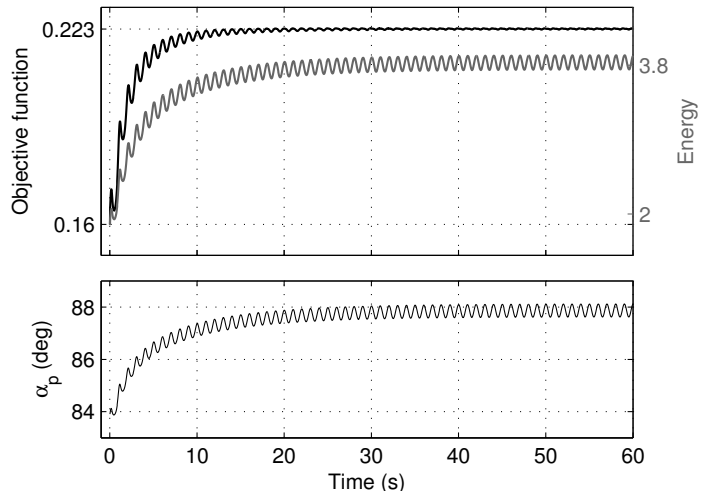


Fig. 7. Extremum-seeking controller for a single parameter ( $\alpha_p$ ) with a fixed birefringence,  $K = 0.1$ .

same as Figure 7. In experiments, the presence of sensor noise may motivate an increase in the amplitude of oscillation  $a$ , a decrease in the frequency of oscillation, or both. Time delays  $\tau$  in the sensing and actuation may be incorporated into the phase delay  $\phi$  according to the formula  $\phi = \tau\omega$  so that the high-pass filtered measurement and input perturbation are aligned. Note that there is no convergence criterion, after which the controller is shut off; even after it converges on the local maximum, the controller continues to adaptively correct for slow disturbances.

TABLE III  
EXTREMUM-SEEKING PARAMETER VALUES (SINGLE-INPUT)

	$\omega$ (rad/s)	$\beta$ (rad)	$\phi$ (rad)	$a$ (deg)	$\omega_h$ (rad/s)	$k$
$\alpha_p$	$2\pi$	$\pi/2$	0	0.5	$2\pi$	10

### B. Multi-Parameter Extremum-Seeking Control for Fixed Birefringence $K$

Figure 8 shows the extremum-seeking controller for the multiple-input, single-output (MISO) case where we are controlling all four polarizer angles simultaneously. The extremum-seeking control parameters are shown in Table IV. The multi-parameter design is more complicated than the single parameter case, and involves first designing single-parameter controllers and then combining them pairwise and modifying until the desired performance is achieved.

The multi-parameter extremum-seeking controller takes longer to converge to a local maximum than the single-parameter case, approximately 2 minutes as opposed to 30 seconds. There are two main reasons for this slower convergence: 1) the angle  $\alpha_1$  is being oscillated more slowly, and 2) as the angles are varied simultaneously, they affect each

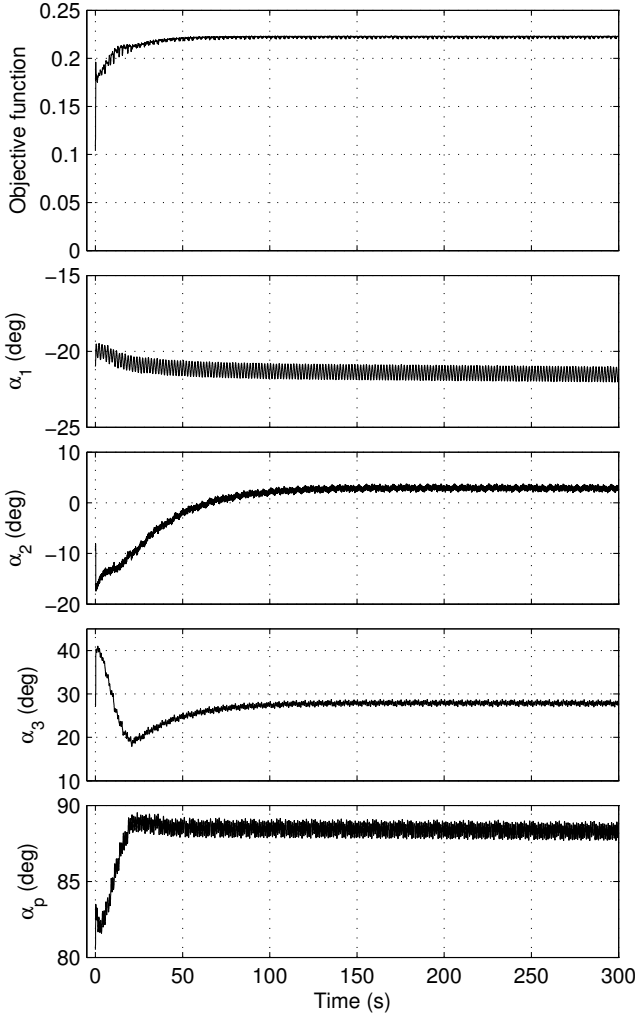


Fig. 8. Multi-parameter extremum-seeking controller with a fixed birefringence,  $K = 0.1$ .

TABLE IV  
EXTREMUM-SEEKING PARAMETER VALUES (MULTI-INPUT)

	$\omega$ (rad/s)	$\beta$ (rad)	$\phi$ (rad)	$a$ (deg)	$\omega_h$ (rad/s)	$k$
$\alpha_1$	$1.2\pi$	0	0	0.5	$2\pi$	5
$\alpha_2$	$4.512\pi$	$\pi/2$	0	0.5	$2\pi$	50
$\alpha_3$	$2\pi$	0	0	0.5	$2\pi$	50
$\alpha_p$	$2\pi$	$\pi/2$	0	0.5	$2\pi$	20

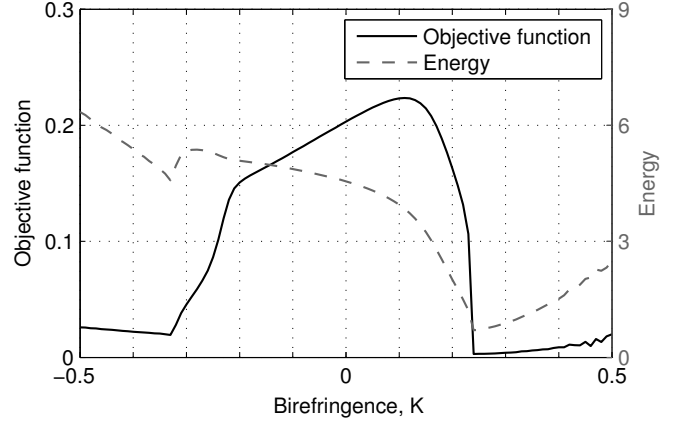


Fig. 9. Energy and objective function vs. birefringence,  $K$ .

other, and larger overall excursion of the angles is required to reach the maximum. Because parameters are all being varied simultaneously at incommensurable rates, occasionally there will be a large excursion in each of the angles, resulting in a large radius in parameter space from the optimal values. Since the mode-locked state is sensitive to large amplitude excursions to the input angles, this may present a challenge to incorporate more input parameters into the extremum-seeking control algorithm.

Finally, it is important to note that for this particular configuration, the extremum-seeking controller performance is sensitive to the control parameters for the  $\alpha_1$  variable. The oscillation frequency for  $\alpha_1$  is chosen to be the slowest frequency and the gain  $k$  is also the smallest among the input angles. If either of these values are increased significantly, then the controller may get stuck in a periodic-orbit configuration where the variable  $\alpha_1$  precesses at a slow rate, while the other variables rapidly adjust to compensate. Although this is not shown, it is quite interesting that during this precession, the objective function remains relatively constant, suggesting that there are a family of favorable mode-locked states parameterized by  $\alpha_1$ . In practice, this might suggest that the variable  $\alpha_1$  is redundant, which is the subject of current investigation.

### C. Multi-Parameter Extremum-Seeking Control for Varying Birefringence $K$

Figure 9 shows the objective function and energy for a range of birefringence  $K$  for a set of fixed input angles; the angles are chosen to (locally) maximize the objective function at  $K = 0.1$  as in Figure 8. On either side of  $K = 0.1$  the objective function decreases, although there is a steep drop-off for larger positive values of  $K$ , corresponding to the loss of mode-locking.

In Figure 10 we vary the birefringence  $K$  according to a large-amplitude saw-tooth pattern (left) and according to a pseudo-random walk (right). In each of these cases, the extremum-seeking controller is compared with the case when no control is applied and the polarizer angles are fixed at

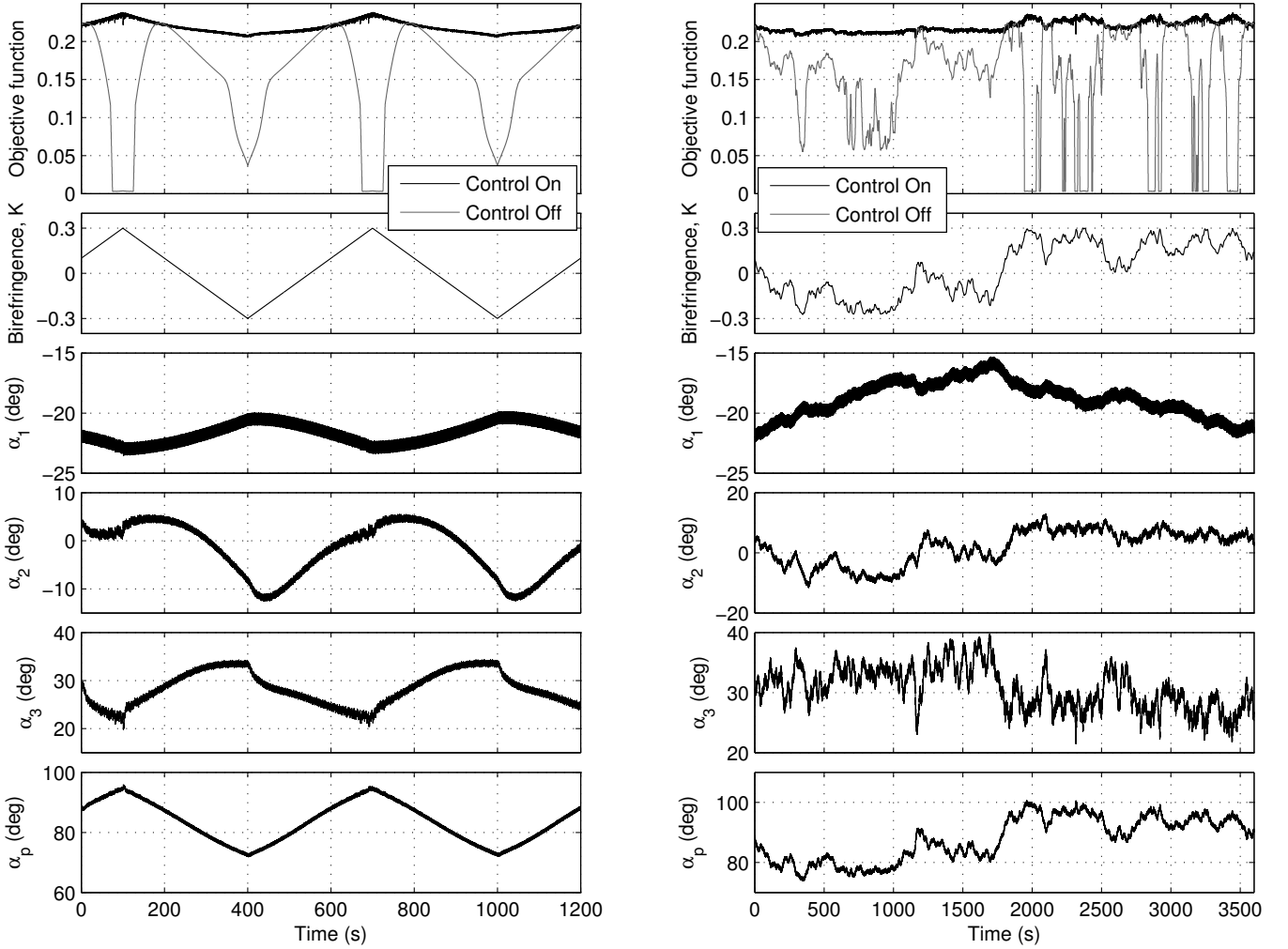


Fig. 10. Multi-parameter extremum-seeking controller with a varying birefringence,  $K$ . (left) The birefringence varies as a sawtooth function, and (right) the birefringence varies according to a pseudo random walk.

the optimal values for  $K = 0.1$ . For both aggressive  $K$  disturbances, the extremum-seeking controller maintains a high-energy mode-locked state, although the uncontrolled system frequently loses mode-locking. It is interesting to note that the fourth input parameter,  $\alpha_p$  tracks the  $K$  disturbance nearly linearly. The objective function fluctuates slightly in the case with controller, since the local maximum value varies with the birefringence  $K$ .

As noted in Table II, the quality of the mode-locked pulse is significantly degraded for an objective function value near 0.1, and the solution is fully chaotic near 0.05. Thus, without control, the laser performance is severely effected by variations in birefringence.

## VI. CONCLUSIONS AND DISCUSSION

We have developed a fast, stable extremum-seeking controller for the passively mode-locked fiber laser based upon NPR. The controller simultaneously varies the four angles corresponding to waveplates and polarizer in a single-NPR

laser to maintain a high-energy mode-locked state despite large, rapid changes in the birefringence  $K$ . The amplitude and frequency of the disturbance are chosen to be more aggressive than expected values, demonstrating that the controller successfully rejects disturbances in a worst-case scenario.

A new objective function was developed for use with the multi-parameter extremum-seeking controller. This objective function divides the energy of a solution by the kurtosis of the Fourier spectrum of the waveform. There are two main criteria for this objective function: 1) high-energy mode-locked states appear as local maxima of the objective function with a buffer between the maxima and chaotic or multi-pulse regions, and 2) it is expressed in terms of experimentally measurable quantities. The objective function developed in this work is not necessarily the only or best function. We might also incorporate quantities such as the average power, full-width at half-maximum of the pulse, or autocorrelation into another objective function depending on specific design goals. It is also possible to use high-frequency sampling to time-average

and reduce measurement noise in experiments.

The control architecture demonstrated in this paper generalizes to multiple-NPR laser systems. However, these systems are extremely expensive to simulate because of the multiple time-scales, especially for a long, time-resolved signal, as in Figures 10. A next-step is to apply these methods in an experiment, and begin increasing the number of NPR sections, which will result in a higher energy pulse. Indeed, the extremum seeking control advocated here may be the only practical way to explore such high-dimensional parameter regimes. The methods in this paper rely on a decent set of starting parameters, so that we are in the attracting basin of a local maximum. For multiple-NPR systems, this parameter space is high-dimensional, and new techniques will need to be developed to identify good starting guesses for the extremum-seeking controller. This may well involve the use of machine learning and data reduction techniques, as in [13].

The extremum-seeking controller may also be used to simply monitor and maintain robust operation of a mode-locked laser. For instance, it may be beneficial to turn on the extremum-seeking controller for a short time to search for the locally optimal parameter values and then fix the angles during operation for improved pulse uniformity. The objective function can be continually monitored, even without perturbing the input parameters, allowing for the construction of a switching criteria to turn on the extremum-seeking controller.

Finally, given the success of the algorithm in the NPR laser, one can easily imagine applying the same techniques to other classes of both solid state and fiber lasers. As long as one can clearly identify parameters which manipulate the mode-locking, then these parameters can be controlled by the algorithm. Alternatively, one can use the algorithm with an objective function that seeks to recover other mode-locking states of interest, whether they be the fastest temporal pulses, pulses with prescribed spectral shapes, etc. Thus it is a general framework that can be easily integrated into practical photonics systems with the potential of great success.

#### ACKNOWLEDGMENTS

J. N. Kutz acknowledges support from the National Science Foundation (NSF) (DMS-1007621) and the U.S. Air Force Office of Scientific Research (AFOSR) (FA9550-09-0174). We would also like to thank F. Wise, W. Renninger and P. Grelu for valuable discussions regarding mode-locking performance.

#### REFERENCES

- [1] K. B. Ariyur and M. Krstić. *Real-Time Optimization by Extremum-Seeking Control*. Wiley, Hoboken, New Jersey, 2003.
- [2] S. Backus, C. G. Durfee, M. M. Murnane, and H. C. Kapteyn. High power ultrafast lasers. *Review of Scientific Instruments*, 69(3):1207–1223, 1998.
- [3] B. G. Bale, K. Kieu, J. N. Kutz, and F. W. Wise. Transition dynamics for multi-pulsing in mode-locked lasers. *Optics Express*, 17(25):23137–23146, 2009.
- [4] P. Binetti, K. B. Ariyur, M. Krstić, and F. Bernelli. Formation flight optimization using extremum seeking feedback. *Journal of Guidance, Control, and Dynamics*, 26(1):132–142, 2003.
- [5] A. I. Bratcu, I. Munteanu, S. Bacha, and B. Raison. Maximum power point tracking of grid-connected photovoltaic arrays by using extremum seeking control. *CEAI*, 10(4):3–12, 2008.

- [6] S. L. Brunton and C. W. Rowley. Maximum power point tracking for photovoltaic optimization using ripple-based extremum seeking control. *IEEE Transactions on Power Electronics*, 25(10):2531–2540, 2010.
- [7] J. Y. Choi, M. Krstić, K. B. Ariyur, and J. S. Lee. Extremum seeking control for discrete-time systems. *IEEE Transactions on Automatic Control*, 47(2):318–323, FEB 2002.
- [8] W. Denk, J. H. Strickler, and W. W. Webb. Two-photon laser scanning fluorescence microscopy. *Science*, 248(4951):73–76, 1990.
- [9] E. Ding and J. N. Kutz. Operating regimes, split-step modeling, and the Haus master mode-locking model. *Journal of the Optical Society of America B*, 26(12):2290–2300, 2009.
- [10] E. Ding, W. H. Renninger, F. W. Wise, P. Grelu, E. Shlizerman, and J. N. Kutz. High-energy passive mode-locking of fiber lasers. *International Journal of Optics*, 2012:1–17, 2012.
- [11] E. Ding, E. Shlizerman, and J. N. Kutz. Generalized master equation for high-energy passive mode-locking: The sinusoidal Ginzburg-Landau equation. *IEEE Journal of Quantum Electronics*, 47(5):705–714, 2011.
- [12] T. Ditmire, J. Zweiback, V. P. Yanovsky, T. E. Cowan, G. Hays, and K. B. Wharton. Nuclear fusion from explosions of femtosecond laser-heated deuterium clusters. *Nature*, 398:489–492, 1999.
- [13] X. Fu and J. N. Kutz. High-energy mode-locked fiber lasers using multiple transmission filters and a genetic algorithm. *Optics Express*, 21(5):6526–6537, 2013.
- [14] H. A. Haus. Mode-locking of lasers. *IEEE Journal of Selected Topics in Quantum Electronics*, 6(6):1173–1185, 2000.
- [15] A. P. Joglekar, H. Liu, G. J. Spooner, E. Meyhöfer, G. Mourou, and A. J. Hunt. A study of the deterministic character of optical damage by femtosecond laser pulses and applications to nanomachining. *Applied Physics B*, 77:25–30, 2003.
- [16] R. C. Jones. A new calculus for the treatment of optical systems. I. description and discussion of the calculus. *Journal of the Optical Society of America*, 31(7):488–493, 1941.
- [17] T. Juhasz. Corneal refractive surgery with femtosecond lasers. *IEEE Journal of Selected Topics in Quantum Electronics*, 5(4):902–910, 1999.
- [18] J. C. Kieffer, A. Krol, Z. Jiang, C. C. Chamberlain, E. Scalzetti, and Z. Ichalalene. Future of laser-based X-ray sources for medical imaging. *Applied Physics B*, 74:S75–S81, 2002.
- [19] A. D. Kim, J. N. Kutz, and D. J. Muraki. Pulse-train uniformity in optical fiber lasers passively mode-locked by nonlinear polarization rotation. *IEEE Journal of Quantum Electronics*, 36(4):465–471, 2000.
- [20] A. Komarov, H. Leblond, and F. Sanchez. Multistability and hysteresis phenomena in passively mode-locked fiber lasers. *Physical Review A*, 71:053809, 2005.
- [21] M. Krstić and H. H. Wang. Stability of extremum seeking feedback for general nonlinear dynamic systems. *Automatica*, 36(4):595–601, April 2000.
- [22] J. N. Kutz. Mode-locked soliton lasers. *SIAM Review*, 48(4):629–678, 2006.
- [23] J. N. Kutz and B. Sandstede. Theory of passive harmonic mode-locking using waveguide arrays. *Optics Express*, 16(2):636–650, 2008.
- [24] R. Leyva, C. Alonso, I. Queinnec, A. Cid-Pastor, D. Lagrange, and L. Martinez-Salamero. Mppt of photovoltaic systems using extremum-seeking control. *Ieee Transactions On Aerospace and Electronic Systems*, 42(1):249–258, January 2006.
- [25] F. Li, E. Ding, J. N. Kutz, and P. K. A. Wai. Dual transmission filters for enhanced energy in mode-locked fiber lasers. *Optics Express*, 19(23):23408–23419, 2011.
- [26] F. Li, P. K. A. Wai, and J. N. Kutz. Geometrical description of the onset of multi-pulsing in mode-locked laser cavities. *Journal of the Optical Society of America B*, 27(10):2068–2077, 2010.
- [27] P. T. Mannion, J. Magee, E. Coyne, G. M. O’Connor, and T. J. Glynn. The effect of damage accumulation behaviour on ablation thresholds and damage morphology in ultrafast laser micro-machining of common metals in air. *Applied Surface Science*, 233:275–287, 2004.
- [28] R. Maury, M. Keonig, L. Cattafesta, P. Jordan, and J. Delville. Extremum-seeking control of jet noise. *Aeroacoustics*, 11(3&4):459–474, 2012.
- [29] C. R. Menyuk. Nonlinear pulse propagation in birefringent optical fibers. *IEEE Journal of Quantum Electronics*, 23(2):174–176, 1987.
- [30] C. R. Menyuk. Pulse propagation in an elliptically birefringent Kerr medium. *IEEE Journal of Quantum Electronics*, 25(12):2674–2682, 1989.
- [31] I. Munteanu, A. I. Bratcu, and E. Ceanga. Wind turbulence used as searching signal for mppt in variable-speed wind energy conversion systems. *Renewable Energy*, 34(1):322–327, January 2009.
- [32] S. Namiki, E. P. Ippen, H. A. Haus, and C. X. Yu. Energy rate equations

for mode-locked lasers. *Journal of the Optical Society of America B*, 14(8):2099–2111, 1997.

- [33] J. Nilsson and D. N. Payne. High-power fiber lasers. *Science*, 332:921–922, 2011.
- [34] Y. Ou, C. Xu, E. Schuster, T. C. Luce, J. R. Ferron, M. L. Walker, and D. A. Humphreys. Design and simulation of extremum-seeking open-loop optimal control of current profile in the DIII-D tokamak. *Plasma Physics and Controlled Fusion*, 50:115001–1–115001–24, 2008.
- [35] M. Pastoor, L. Henning, B. R. Noack, R. King, and G. Tadmor. Feedback shear layer control for bluff body drag reduction. *Journal of Fluid Mechanics*, 608:161–196, 2008.
- [36] B. Ren, P. Frihauf, R. J. Rafac, and M. Krstić. Laser pulse shaping via extremum seeking. *Control Engineering Practice*, 20:674–683, 2012.
- [37] W. H. Renninger, A. Chong, and F. W. Wise. Dissipative solitons in normal-dispersion fiber lasers. *Physical Review A*, 77(2):023814–1–023814–4, 2008.
- [38] W. H. Renninger, A. Chong, and F. W. Wise. Self-similar pulse evolution in an all-normal-dispersion laser. *Physical Review A*, 82:021805, 2010.
- [39] W. H. Renninger, A. Chong, and F. W. Wise. Pulse shaping and evolution in normal-dispersion mode-locked fiber lasers. *IEEE Journal of Selected Topics in Quantum Electronics*, 18(1):389–398, 2012.
- [40] D. J. Richardson, J. Nilsson, and W. A. Clarkson. High power fiber lasers: current status and future perspectives. *Journal of the Optical Society of America B*, 27(11):B63–B92, 2010.
- [41] X. Shen, W. Li, M. Yan, and H. Zeng. Electronic control of nonlinear-polarization-rotation mode locking in Yb-doped fiber lasers. *Optics Letters*, 37(16):3426–3428, 2012.
- [42] S. Toyran, Y. Liu, S. Singha, S. Shan, M. R. Cho, R. J. Gordon, and D. P. Edward. Femtosecond laser photodisruption of human trabecular meshwork: an in vitro study. *Experimental Eye Research*, 81:298–305, 2005.
- [43] A. Vogel, J. Noack, G. Hüttman, and G. Paltauf. Mechanisms of femtosecond laser nanosurgery of cells and tissues. *Applied Physics B*, 81:1015–1047, 2005.
- [44] A. Vogel and V. Venugopalan. Mechanisms of pulsed laser ablation of biological tissues. *Chemical Reviews*, 103(2):577–644, 2003.
- [45] H. H. Wang, M. Krstić, and G. Bastin. Optimizing bioreactors by extremum seeking. *Adaptive Control and Signal Processing*, 13(8):651–669, 1999.
- [46] H. H. Wang, S. Yeung, and M. Krstić. Experimental application of extremum seeking on an axial-flow compressor. *IEEE Transactions on Control Systems Technology*, 8(2):300–309, 2000.
- [47] C. Xu and W. W. Webb. Measurement of two-photon excitation cross sections of molecular fluorophores with data from 690 to 1050 nm. *Journal of the Optical Society of America B*, 13(3):481–491, 1996.
- [48] A. H. Zewail. Femtochemistry: past, present, and future. *Pure and Applied Chemistry*, 72(12):2219–2231, 2000.
- [49] C. Zhang and R. Ordonez. Numerical optimization-based extremum seeking control with application to ABS design. *IEEE Transactions on Automatic Control*, 52(3):454–467, 2007.



mathematics at the University of Washington.

**Steven L. Brunton** received the B.S. degree in mathematics with a minor in control and dynamical systems from the California Institute of Technology, Pasadena, CA, in 2006, and the Ph.D. degree in mechanical and aerospace engineering from Princeton University, Princeton, NJ, in 2012. He is currently an Acting Assistant Professor of applied



**Xing Fu** received the B.S. degree in applied mathematics from the Sichuan University, Chengdu, Sichuan, China, in 2009, and a M.S. degree in applied mathematics from the University of Washington, Seattle, WA, in 2010. He is currently working toward the Ph.D. degree in applied mathematics at the University of Washington, Seattle, WA.



**J. Nathan Kutz** received the B.S. degrees in physics and mathematics from the University of Washington, Seattle, WA, in 1990, and the Ph.D. degree in applied mathematics from Northwestern University, Evanston, IL, in 1994. He is currently a Professor and Chair of applied mathematics at the University of Washington.